

# High-resolution x-ray spectromicroscopy with the Tokyo electron beam ion trap

N. Nakamura<sup>a)</sup>

*Cold Trapped Ions Project, ICORP, Japan Science and Technology Corporation (JST), Chofu, Tokyo 182-0024, Japan*

A. Ya. Faenov and T. A. Pikuz

*Multicharged Ions Spectra Data Center, National Institute for Physical-Technical and Radiotechnical Measurements, Moscow Region, 141570, Russia*

E. Nojikawa

*Cold Trapped Ions Project, ICORP, Japan Science and Technology Corporation (JST), Chofu, Tokyo 182-0024, Japan*

H. Shiraishi

*Institute for Laser Science, The University of Electro-Communications, Tokyo 182-8585, Japan*

F. J. Currell<sup>b)</sup> and S. Ohtani<sup>b)</sup>

*Cold Trapped Ions Project, ICORP, Japan Science and Technology Corporation (JST), Chofu, Tokyo 182-0024, Japan*

(Received 12 May 1998; accepted for publication 24 November 1998)

A high-resolution x-ray spectrometer with a spherically bent quartz crystal and an x-ray sensitive charge coupled device (CCD) have been applied to the observation of highly charged ions produced and trapped in the Tokyo electron beam ion trap (EBIT). The spectrometer made it possible to measure the spatial distribution and wavelength of the radiation at the same time. A simple, but lower energy resolution method was also used, by taking advantage of the intrinsic energy resolution of the CCD. The possibility to apply such techniques to diagnostics of an EBIT is discussed. © 1999 American Institute of Physics. [S0034-6748(99)00103-3]

## I. INTRODUCTION

It has been demonstrated during the past several years that an electron beam ion trap (EBIT)<sup>1</sup> is a unique source for the production<sup>2</sup> and spectroscopy<sup>3</sup> of highly charged ions. One of the important tasks in investigations with an EBIT is the diagnostics of EBIT source parameters, such as the size of the source. Knapp *et al.* measured the radial size of the source of x-ray radiation from super-EBIT<sup>4</sup> using an x-ray pinhole camera. Since the radiation occurs within the region of interaction between the trapped ions and the electron beam, the radial size of the source of x-ray radiation is considered to give the radius of the electron beam. This radius is related to a very important parameter, the electron beam current density.

It is also important to measure the vertical size of the radiation source. Crespo López-Urrutia *et al.*<sup>5,6</sup> observed visible transitions in Xe ions trapped in super-EBIT and found that the vertical size of the source of radiation for highly charged ions differs from that for neutral atoms. Therefore, measurements of the vertical size may help to assign observed peaks. In addition measurements of the vertical size can give information about the temperature of

trapped ions. Schneider *et al.*<sup>7</sup> measured the vertical ion distribution in an EBIT and deduced the temperature of the ions. However, measurement of the vertical size of x-ray radiation simultaneously with high energy resolution has not been performed yet. It allows one to measure ion distributions for different charge states. Such measurement can be made by obtaining x-ray spectra of highly charged ions with spatial resolution.<sup>8</sup> In principle, for such measurements any x-ray crystal spectrometer can be used if a slit is placed before or after the crystal in the direction parallel to the dispersion of the crystal.<sup>9,10</sup> However, since the luminosity of such a scheme is very small, it is practically impossible to use such a scheme for a weak source, such as an EBIT. This method can be used however with an x-ray sensitive charge coupled device (CCD), since this detector provides simultaneous intrinsic energy resolution and spatial resolution. The final energy resolution in such a setup is determined by the rather poor (typically  $\sim 300$  eV) energy resolution of the CCD. For higher energy resolution, we used spherically bent crystals in the focusing spectrometer with spatial resolution [FSSR-1 two-dimensional (2D)] scheme<sup>11-13</sup> to obtain the spatial distribution of radiation. It allows one to receive highly resolved ( $\lambda/\Delta\lambda \sim 10\,000$ ) x-ray spectra simultaneously with high spatial (up to  $4\ \mu\text{m}$ ) resolution and very high luminosity. First results with Ne-like Ba ions are described in this article.

<sup>a)</sup>Electronic mail: nakamura@hci.jst.go.jp

<sup>b)</sup>Also at: Institute for Laser Science, The University of Electro-Communications, Tokyo 182-8585, Japan.

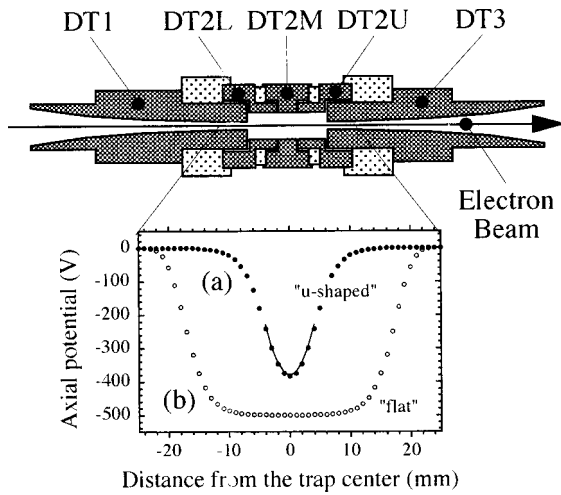


FIG. 1. Trap region of the Tokyo EBIT. The trap consists of five electrodes, DT1, 2L, 2M, 2U, and 3. The calculated axial potentials are shown for (a) u-shaped potential which is achieved by applying  $-500$  V to DT2M with respect to DT1, 2L, 2U, and 3; (b) flat potential which is achieved by applying  $-500$  V to all of the DT2 electrodes with respect to DT1 and 3. The solid line represents the harmonic potential curve fitted to the potential (a) for the region of  $|z| \leq 4$  mm.

**II. EXPERIMENTAL SETUP**

**A. The Tokyo EBIT**

A detailed description of the Tokyo EBIT has been given in previous articles.<sup>14-16</sup> Briefly, the device consists of three parts, an electron gun, a cryostat region including drift tubes, and an electron collector. The electrons emitted from the electron gun are accelerated upwards by the potential difference between the electron gun and the drift tubes, while being magnetically compressed. The resultant beam ionizes and traps ions in the drift tube region, shown in Fig. 1. In the present set of experiments, the observations were performed with two different trap potential shapes to demonstrate how the spectrometer works as an imaging device. One of them is a “flat” trap potential which was achieved by applying negative potential to all of the DT2 electrodes [DT2L, M, and U] with respect to DT1 and 3, while the other one is a “u-shaped” trap potential which was achieved by applying negative potential only to DT2M with respect to DT1, 2L, 2M, and 3. The axial potentials for both conditions which are calculated with SIMION<sup>17</sup> are shown in Fig. 1. In the calculation the space charge potential due to the electron beam is neglected. Since the beam radius and velocity were almost constant along the trap, the effect of space charge was to shift the whole potential distribution along the trap by a constant amount, but not change the shape. The ion distribution along the electron beam is not expected to be flat when a u-shaped potential is adopted, while it is expected to be flat when a flat potential is adopted. At the center of the drift tubes, there are eight slits 10 mm long (in a direction parallel to the electron beam) and 2 mm wide (in a direction perpendicular to the electron beam), which are used for observation, neutral gas injection, and laser introduction. After exiting the drift tubes, the electron beam is decelerated by the potential difference between the drift tubes and the collector, and then collected by the electron collector. The electron beam energy

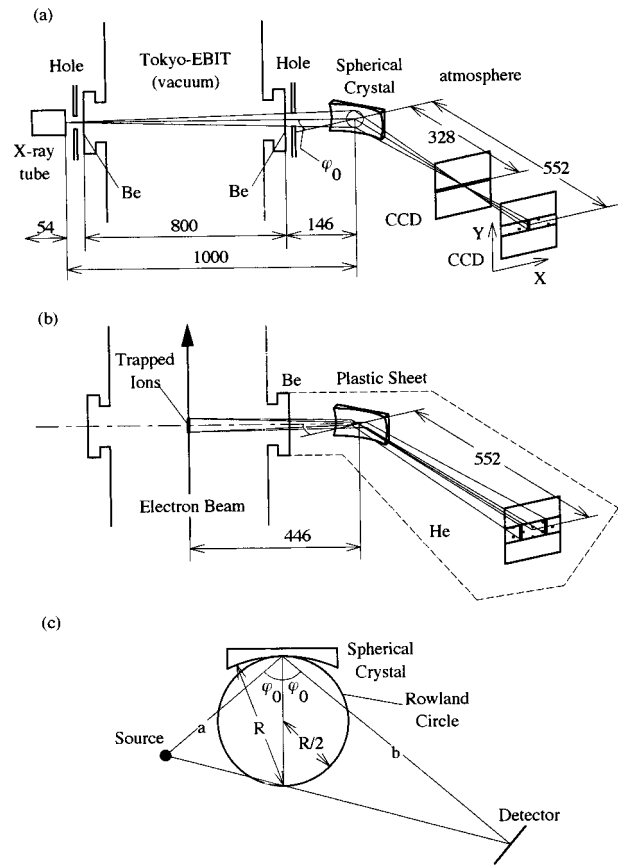


FIG. 2. Schematic drawings of the experimental setup. (a) The arrangement for the alignment procedure; (b) the arrangement for the observation of radiation from the EBIT; (c) the schematic drawing of the FSSR-2D scheme. The notations in (c) are given in the text.

and current were set to 7.4 keV and 120 mA, respectively to produce Ne-like Ba ( $Ba^{46+}$ ). Ba was evaporated from the cathode and ionized in the trap region. The trapped ions were periodically dumped once per 60 s. No coolant<sup>18</sup> was injected during the measurements.

**B. Spectrometer**

For investigation of radiation from the EBIT, a spherically bent crystal, placed in a FSSR-2D configuration<sup>9,11</sup> was used (see Fig. 2). In such a scheme the spherical crystal is placed on the Rowland circle, while the x-ray source and the detector are placed out of the Rowland circle. The parameters of this scheme are defined by the following equations. The angle of incidence  $\varphi_0$  is given by

$$\varphi_0 = 90^\circ - \arcsin \frac{m\lambda_0}{2d}, \tag{1}$$

where  $\lambda_0$  is the central wavelength of the spectral range,  $d$  is the lattice spacing of the crystal, and  $m$  is the order of diffraction. The distance  $a$  between the source and the crystal is given by

$$a = \frac{R(M_s + 1)}{2M_s \cos \varphi_0}, \tag{2}$$

where  $M_s$  is the linear magnification in the sagittal plane and  $R$  is the radius of curvature of the crystal. The distance  $b$  between the crystal and the plane of sagittal beam focusing (detector position) is given by

$$b = \frac{aR}{2a \cos \varphi_0 - R}. \quad (3)$$

Linear magnification  $M_m$  in the plane of the dispersion (meridional) plane is given by

$$M_m = \frac{R[a - \cos \varphi_0(2a \cos \varphi_0 - R)]}{(R \cos \varphi_0 - a)(2a \cos \varphi_0 - R)}. \quad (4)$$

For measurements of  $n=3$  to 2 transitions in Ne-like Ba (wavelength about 2.5 Å) we used a spherically bent quartz crystal (orientation  $2d=6.67$  Å) with a radius of curvature of 186 mm and working area size of  $50 \times 15$  mm<sup>2</sup>. This orientation has the biggest reflectivity when compared to other orientations of quartz and the working angle ( $\varphi_0=67.7^\circ$ ) is still very reasonable.

To increase the luminosity, it was necessary to place the crystal as close to the source as possible. Therefore the crystal was placed just after the Be window, which separates the vacuum of the EBIT and the atmosphere. The distance  $a$  between the EBIT source and the crystal was 446 mm (see Fig. 2). Using Eqs. (1)–(4) we determined the parameters  $b$ ,  $M_s$ , and  $M_m$  to be 552 mm, 1.24, and 1.28, respectively. An x-ray CCD was used as a detector for the spectrometer in this experiment as described in Sec. IID.

To prevent absorption of the radiation by air, the spectrometer was surrounded by a plastic sheet and the air inside of the sheet was replaced by helium gas during observation with the EBIT [see Fig. 2(b)]. Helium gas which was always evaporating from the liquid helium vessel in the EBIT was used to fill the region inside the sheet. The CCD was cooled to liquid nitrogen temperature to decrease thermal noise. To prevent ice from forming on the CCD, it was operated in vacuo and a Be foil with a thickness of 500 μm was used to separate the vacuum of the CCD chamber from the atmosphere, although the chamber is not shown in Fig. 2.

### C. Alignment procedure

To obtain good spectral and spatial resolution the FSSR spectrometer must be aligned very carefully. Due to some analogies between reflections of x-ray radiation and visual light, usually a visible point source can be used for the precise alignment of the spherically bent crystal spectrograph by putting it in the plane of the x-ray source. However, in the case of the EBIT source such a method could not easily be used since it is difficult to put such a source at the center of the drift tubes. In such a case an x-ray tube with a radiation wavelength close to the radiation to be investigated can be used. As shown in Fig. 2(a), an x-ray tube with a Ti target was placed on the axis, through the center of the two Be windows and the center of the EBIT. For collimation of x-ray radiation two apertures with diameters of 5 mm were mounted just after the Be windows (the distance between these apertures was about 850 mm). This scheme allowed us to illuminate the central zone (diameter of about 6 mm) of the spherical crystal. Emission of K-β line of Ti ( $\lambda=2.514$

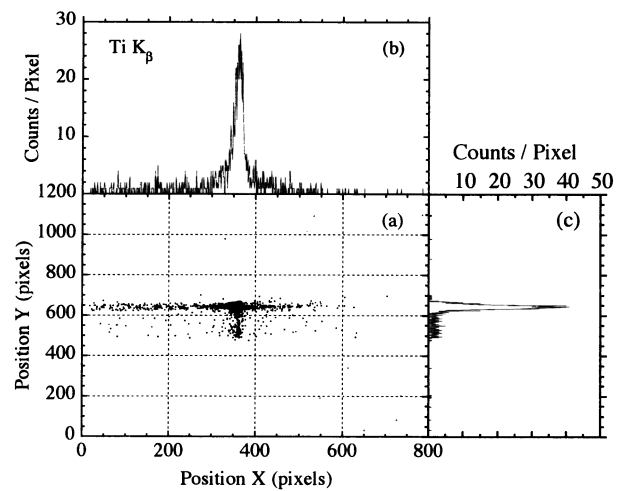


FIG. 3. Spatially resolved x-ray spectrum of Ti  $K\beta$  line radiated from the x-ray tube. The distance between the crystal and the detector was 328 mm [see Fig. 2(a)]. (a) The two-dimensional image on the CCD; (b) the integrated image for the vertical direction, i.e., x-ray spectrum obtained by the crystal dispersion; (c) the integrated image for the horizontal direction, i.e., spatial distribution of the radiation.

Å) was chosen for alignment because the wavelength of this line is very close to that of  $(2p_{3/2})^{-1}(3d_{5/2})_1 - 2p^6$  transition of Ne-like Ba ( $\lambda=2.512$  Å).

Emission of the K-β line reflected by the crystal was observed by the x-ray CCD at two different distances from the crystal; the best focus position for the x-ray tube source ( $a=1000$  mm,  $b=328$  mm) and that for the EBIT source ( $b=552$  mm). Figure 3(a) shows a two-dimensional image from the CCD taken with  $b=328$  mm. The horizontal axis ( $X$ ) corresponds to the direction of the spectral dispersion, while the vertical axis ( $Y$ ) corresponds to the direction of the spatial resolution. Figures 3(b) and 3(c) represent the integrated image for the vertical and horizontal directions, respectively, i.e., Fig. 3(b) represents x-ray spectrum obtained by the crystal dispersion and 3(c) spatial distribution of the tube source. Since x rays from the tube were well collimated, only K-β can be observed and K-α cannot be observed. Since the size of the x-ray tube source was small (about 300 μm), it is assumed that we can estimate spatial resolution, which could be obtained with the spectrometer in our experiment. As follows from Fig. 3(c) the size of the x-ray source image was 0.45 mm. This means that in the present case, when  $M_s$  was equal to 0.3, we had spatial resolution in the sagittal plane of better than 1.5 mm.

Figure 4 shows a similar picture as Fig. 3, but for  $b=552$  mm. Since the arrangement was not the best focus condition for the tube, the broad spatial distribution is seen in Fig. 4(c). A comparison between Figs. 3 and 4 might help one to understand how the spectrometer works as an imaging device. The position of K-β line in Fig. 4 shows the area where the spectra of Ne-like Ba lines is expected. The alignment procedure described above was efficient for both the angle and space alignment of a FSSR-2D spectrograph applied to an EBIT source.

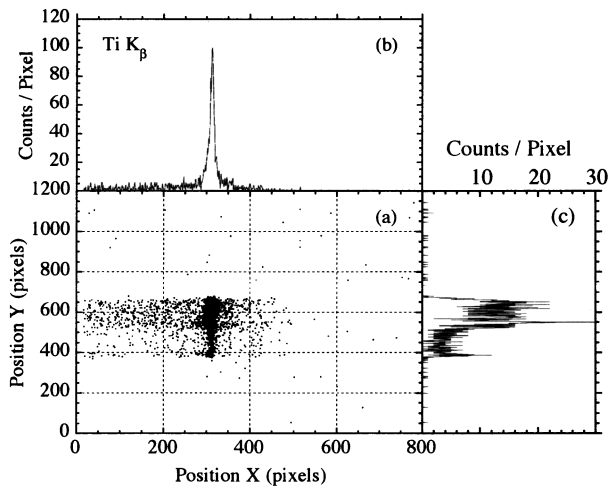


FIG. 4. Similar to Fig. 3, however the distance between the crystal and the detector was 552 mm [see Fig. 2(a)].

#### D. X-ray detector

As described above, an x-ray sensitive CCD was used as a detector<sup>19</sup> for the spectrometer in this experiment, while a position sensitive proportional counter (PSPC) is commonly used in spectroscopic studies with an EBIT. There are two ways to detect x rays with a CCD. One is to place a fluorescent screen in front of a conventional visible CCD, another is to directly detect x rays with a CCD specially produced for x-ray detection. The latter is called the direct x-ray detection method,<sup>20</sup> and was used in the present experiment. This method has an advantage in that the number of electron-ion pairs, i.e., the pulse height of the signal, gives the energy of the x-ray photon. Therefore, it can be said that an x-ray CCD has good spatial resolution and energy resolution at the same time. The characteristics of the CCD used in the measurements are summarized in Table I. The difference between an x-ray CCD and a conventional visible CCD is the depth of the depletion layer. To detect x rays with high sensitivity, the depletion layer should be thick compared with that of a visible CCD. Spatial resolution of an x-ray CCD is determined by the pixel size, which was  $22.5 \times 22.5 \mu\text{m}^2$  in this case, while typical spatial resolution of a PSPC is about 100–300  $\mu\text{m}$ . For observations with an EBIT, since the electron beam diameter which acts as the input slit for a spectrometer is typically 60  $\mu\text{m}$ , in most cases where a PSPC is used as a detector total spectral resolution is determined by spatial resolution of a detector.<sup>21</sup> Although in the observation by Beiersdorfer *et al.*<sup>22</sup> the spectral resolution was limited by the thermal Doppler width and the natural width, the observation needed large dispersion, i.e., a spectrometer of a large size. Since the spatial resolution of a CCD is smaller than the

TABLE I. Characteristics of the x-ray CCD used in the experiment.

Product number	EEV CCD05-20-5-207
Pixel number	$1152 (V) \times 770 (H)$
Effective area	$25.9 \times 17.3 \text{ mm}^2$
Pixel size	$22.5 \times 22.5 \mu\text{m}^2$
Thickness of the depletion layer	50 $\mu\text{m}$
Energy resolution at $\sim 5 \text{ keV}$	300 eV (typical)

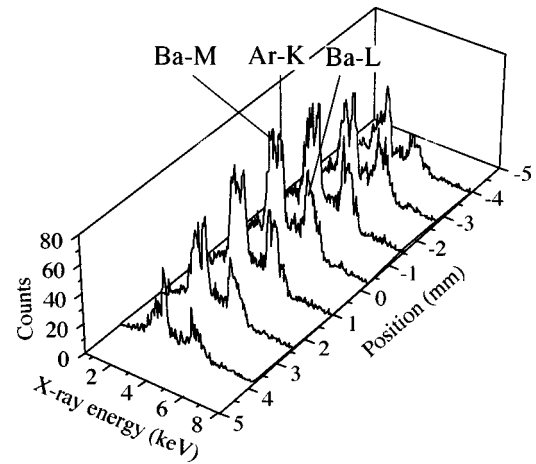


FIG. 5. Spatially resolved x-ray spectrum taken with a slit and an x-ray CCD. “Ba-M” and “Ba-L” represent M and L lines of Ba ions, respectively, while “Ar-K” represents K lines of Ar ions.

electron beam diameter, spectral resolution can be improved by using a CCD as a detector while keeping size of the spectrometer small. In addition, since energy resolution of an x-ray CCD is as high as a solid state detector, it is possible to significantly increase the signal to background ratio by excluding signals which have undesired energies during analysis. Since a CCD is position sensitive in two dimensions, the signal to background ratio can be improved by selecting the region where the real signals appear, perpendicular to the dispersive direction.

We also used the CCD to perform low energy resolution imaging experiments directly. A slit with a width of 0.5 mm was placed between the electron beam and the CCD, perpendicular to both the electron beam and a line joining it to the CCD. The distance between the electron beam and the slit was about 555 mm and the distance between the slit and the CCD was about 900 mm. With this setup, the spatial distribution of the radiation along the direction parallel to the electron beam was obtained with a magnification of about 1.6 and a spatial resolution of about 1.3 mm. The x-ray energy was determined from the pulse height of the CCD output. The voltage of  $-100 \text{ V}$  was applied to DT2M with respect to DT1, 2L, 2U, and 3 during the experiment.

### III. RESULTS AND DISCUSSION

Figure 5 shows the results for the low energy resolution imaging experiments described in Sec. II D. Ar gas was injected through the side port during the experiment while Ba was evaporated from the cathode and ionized in the trap. As shown in the figure, the spatial distribution is narrower for Ba ions than that for Ar ions. If the temperature of trapped ions reaches equilibrium, the spatial distribution becomes narrower for higher charge states of the trapped ions because the trapping potential becomes larger. This is consistent with the present result since it is assumed that the dominant charge state was  $46+$  for Ba and  $18+$  for Ar under the present experimental conditions. In plasmas, elements which have different atomic numbers reveal different spatial distributions.<sup>11</sup> Thus the observation of the spatial distribution is considered to be very useful in the diagnostics of

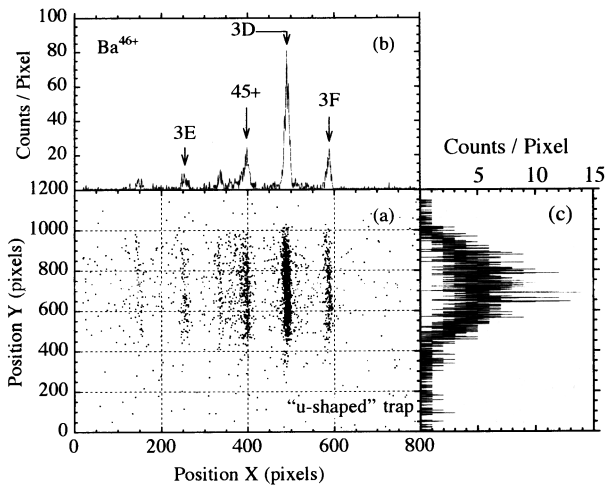


FIG. 6. Similar to Fig. 4, however Ne-like Ba trapped in the EBIT was observed [see Fig. 2(b)]. The u-shaped trap potential was adopted during the observation [see Fig. 1(a)].

plasmas which contain several kinds of elements. Even if a plasma is formed by ions of only one element, spatial distributions for ions with different charge states can be different. To observe the spatial distributions for different charge states, higher energy resolution imaging experiments would need to be performed to resolve radiation from ions with different charge states. For this purpose, the FSSR schemes are very useful.

Figure 6 shows a similar spectrum to Fig. 4, but L lines of Ne-like Ba trapped in the EBIT were observed. The u-shaped trap potential was applied to the trap. Several L lines correspond to  $n=3$  to 2 transitions are shown in Fig. 6(b). The notations in the figure are the same as those used by Beiersdorfer *et al.*<sup>23</sup> Good spectral resolution has been obtained compared with the observations by Marrs *et al.*<sup>1</sup> and Chantler *et al.*<sup>24</sup> Spectral dispersion for the present setup was about  $6 \times 10^{-3}$  Å/mm or  $1.4 \times 10^{-4}$  Å/pxl. This means that the nominal spectral resolution  $\lambda/\Delta\lambda$  for a point source which could be achieved was about 18 000. The source size of the EBIT, i.e., the diameter of the electron beam, is calculated to be about  $60 \mu\text{m}$  by Herrmann's theory.<sup>25</sup> The magnification in the meridional plane (in the direction of spectral dispersion) in the present experiment was about 1.3. This means that in the plane of dispersion there was a width of about  $80 \mu\text{m}$  due to the source size. Having taken into account the source size it was estimated that the nominal spectral resolution in the present experiment was 4500. Position resolution, i.e., pixel size of the CCD, did not affect the spectral resolution since it was small compared to the diameter of the electron beam. Although the absolute values of the transition wavelengths are not determined in the present experiments, they can be obtained by observing several reference lines as Cowan *et al.*<sup>26</sup> did for the precision measurement of the transition energy in Na-like platinum ions.

Figure 7 shows a similar spectrum to that of Fig. 6, however the flat potential was applied to the trap. As expected, the spatial distribution of the radiation is flat for Fig. 7(c) and not flat for Fig. 6(c), while the dispersion spectra

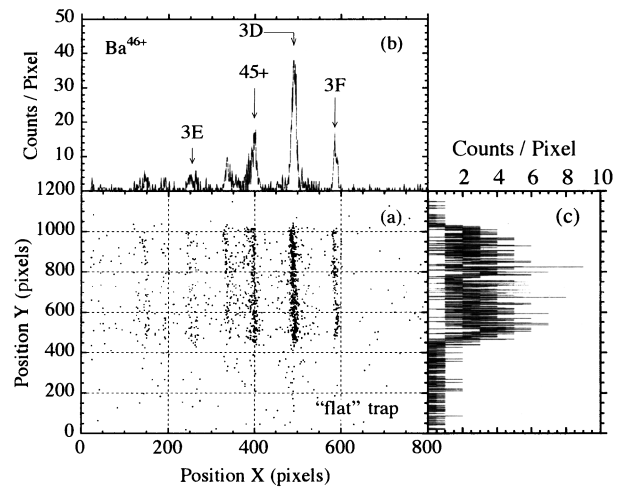


FIG. 7. Similar to Fig. 5, however, the flat trap potential was adopted during the observation [see Fig. 1(b)].

[Figs. 6(b) and 7(b)] are practically the same. In both cases, the length of the base of the spatial distribution is about 12 mm on the CCD, which corresponds to 10 mm at the EBIT source. This is considered to be the whole observable region since the height of the observation slit at the trap region is 10 mm. From the spatial distribution of the trapped ions, it is possible to have information for important parameters of the EBIT.

For the u-shaped trap potential, since the ions become more concentrated in the central region of the trap as the temperature of the ions reduces, we can get information about the temperature of the observed ions. Beiersdorfer *et al.*<sup>21</sup> measured the temperature of the ions trapped in an EBIT by observing the spectral line width. Since the temperature of ions trapped in an EBIT is so low that the Doppler broadening effect is small, a spectrometer with a very high resolution ( $\lambda/\Delta\lambda > 20\,000$ ) should be employed to determine the temperature from the linewidth. This makes the luminosity low and many hours would be needed for good statistics, while the present method does not need such high spectral resolution and the luminosity is kept high.

The temperature of the trapped ions can be derived from the present measurement as follows. Assuming that the trapped ions follow the Maxwell-Boltzmann distribution for a temperature  $T$ , the number density of the ions at the position  $(r, z)$  is represented as

$$n(r, z) dr dz = A (MkT)^{3/2} \exp\left[-\frac{qV(r, z)}{kT}\right] dr dz, \quad (5)$$

where  $A$  is a constant,  $M$  is the mass of the trapped ions,  $k$  is the Boltzmann constant,  $q$  is the charge state of the ions, and  $V$  is the potential at the position  $(r, z)$ . The ion distribution along the  $z$  axis is obtained by integration of Eq. (5) with respect to  $r$ ,

$$n(z) dz = A (MkT)^{3/2} \left\{ \int_0^p 2\pi r \exp\left[-\frac{qV(r, z)}{kT}\right] dr \right\} dz, \quad (6)$$

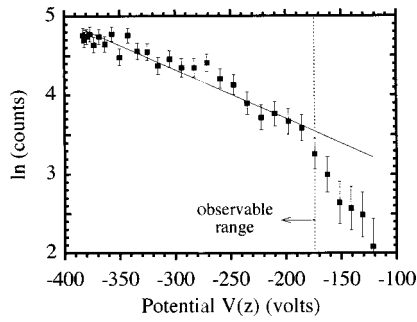


FIG. 8. The natural logarithm of the x-ray intensity observed from a small section of the trap along the  $z$  axis as a function of the local potential in that section as determined from Fig. 1. The result of fitting to a linear function for the potential in the observable region is shown by the solid line.

where  $\rho$  is the radius of the drift tube. Since the trap configuration is axially symmetric, the potential inside the trap is given by

$$V(r, z) = \alpha_0 + \alpha_2(2z^2 - r^2) + \alpha_4(8z^4 - 24z^2r^2 + 3r^4) + \dots, \quad (7)$$

where  $\alpha_k$  are constants. Near the center of the trap, the first and the second terms in Eq. (7) are dominant, i.e., the potential is considered to be approximated as a harmonic potential. The calculated potential in the region of  $|z| \leq 4$  mm was fitted to a harmonic potential, and the result is shown in Fig. 1 by the solid line. Good agreement between the fitted curve and the calculated potential indicates that the first and the second terms in Eq. (7) are dominant for this region. Consequently, the potential at the center of the trap can be approximated as

$$V(r, z) = V(r) + V(z). \quad (8)$$

By introducing Eq. (8) and Eq. (6), the number density of the ions is represented as

$$\begin{aligned} n(z)dz &= A(MkT)^{3/2} \\ &\times \left\{ \int_0^\rho 2\pi r \exp\left[-\frac{qV(r) + qV(z)}{kT}\right] dr \right\} dz \\ &= A(MkT)^{3/2} \left\{ \int_0^\rho 2\pi r \exp\left[-\frac{qV(r)}{kT}\right] dr \right\} \\ &\times \exp\left[-\frac{qV(z)}{kT}\right] dz \\ &= B(M, T, q) \exp\left[-\frac{qV(z)}{kT}\right] dz, \end{aligned} \quad (9)$$

where  $B$  is a function which is dependent on  $M$ ,  $T$ , and  $q$  but is independent of  $z$ . By taking the natural logarithm of Eq. (9), the following relation is obtained:

$$\ln[n(z)] = \ln[B] - \frac{qV(z)}{kT}. \quad (10)$$

Therefore it is expected that the logarithm of the x-ray intensity is linear dependent on the potential, and the gradient is  $-q/kT$ .

Figure 8 shows the dependence of the logarithm of the x-ray intensity upon the axial potential. For this plot, the

calculated potential shown in Fig. 1 was used. As expected, a linear dependence is found for the observable range (about  $\pm 5$  mm as determined by the slot in the drift tubes). The x-ray signals observed outside the observable range are considered to be contributions arising from background, the uncertainty of the absolute position, and the position resolution of the spectrometer. The gradient of the fitted line is  $6.2 \times 10^{-3} [\text{V}^{-1}]$ , which corresponds to  $7.5 \pm 3.5$  keV for  $q=46$ . The uncertainty was estimated from the statistics, the uncertainty in the determination of the absolute position, and spatial resolution of the spectrometer. Since the axial trap potential  $V_{\text{trap}}$  was about 380 V for the u-shaped trap,  $T/qV_{\text{trap}}$  is about 0.4. Although the present result is consistent with the results obtained by Schneider *et al.*,<sup>7</sup> the temperature obtained from the present measurement is much higher than that obtained by Beiersdorfer *et al.*<sup>21,22</sup> and by Adler *et al.*<sup>27</sup> The present method, which is similar to the method adopted by Schneider *et al.*, might give a higher value. In addition, the absence of coolant can obviously result in higher temperature. The axial trap potential  $V_{\text{trap}}$ , which is larger than the previous experiments can also result in higher temperature. The larger magnetic field can also result in higher temperature since the electron current density increases with the magnetic field, and thus the collision rate, i. e., the heating rate by the electron collision increases. When the trap is operated in the conventional mode, i. e., the same potential is applied to all of DT2L, M, and U, we cannot have any information about temperature because the spatial distribution should be always flat.

## ACKNOWLEDGMENT

The authors thank Dr. Y. Aglitskiy for fruitful discussions about using focusing spectrographs for EBIT experiments. We also thank Ann Currell for help in preparing this manuscript.

<sup>1</sup>R. E. Marrs, M. A. Levine, D. A. Knapp, and J. R. Henderson, Phys. Rev. Lett. **60**, 1715 (1988).

<sup>2</sup>R. E. Marrs, S. R. Elliott, and D. A. Knapp, Phys. Rev. Lett. **72**, 4082 (1994).

<sup>3</sup>P. Beiersdorfer, G. V. Brown, J. Crespo López-Urrutia, V. Decaux, S. R. Elliott, D. W. Savin, A. J. Smith, G. S. Stefanelli, K. Widmann, and K. L. Wong, Hyperfine Interact. **99**, 203 (1996).

<sup>4</sup>D. A. Knapp, R. E. Marrs, S. R. Elliott, E. W. Magee, and R. Zasadzinski, Nucl. Instrum. Methods Phys. Res. A **334**, 305 (1993).

<sup>5</sup>José R. Crespo López-Urrutia, P. Beiersdorfer, K. Widmann, and V. Decaux, XIX International Conference on The Physics of Electronic and Atomic Collisions, Whistler, Canada, Abstract book, 1995 (unpublished), Vol. II, p. 589.

<sup>6</sup>José R. Crespo López-Urrutia, P. Beiersdorfer, K. Widmann, and V. Decaux, Annual Report 1995 (EBIT, N-Division Experimental Physics, 1996 (unpublished), p. 26.

<sup>7</sup>M. B. Schneider, M. A. Levine, C. L. Bennett, J. R. Henderson, D. A. Knapp, and R. E. Marrs, in *International Symposium on Electron Beam Ion Sources and Their Applications, Proceedings of the International Symposium held on Electron Beam Ion Sources and their Applications at the Brookhaven National Laboratory, Upton, 1988*, AIP Conf. Proc. No. 188, edited by A. Hershcovitch (AIP, New York, 1989), p. 158.

<sup>8</sup>V. A. Boiko, A. V. Vinogradov, S. A. Pikuz, I. Yu. Skobelev, and A. Ya. Faenov, J. Sov. Laser Res. **6**, 85 (1985).

<sup>9</sup>T. A. Pikuz, A. Ya. Faenov, S. A. Pikuz, V. M. Romanova, and T. A. Shelkovenko, J. X-Ray Sci. Technol. **5**, 323 (1995).

<sup>10</sup>I. Yu. Skobelev, A. Ya. Faenov, B. A. Bryunetkin, V. M. Dyakin, T. A.

- Pikuz, S. A. Pikuz, T. A. Shelkovenko, and V. M. Romanova, *JETP* **81**, 692 (1995).
- <sup>11</sup>A. Ya. Faenov, S. A. Pikuz, A. I. Erko, B. A. Bryunetkin, V. M. Dyakin, G. V. Ivanenkov, A. R. Mingaleev, T. A. Pikuz, V. M. Romanova, and T. A. Shelkovenko, *Phys. Scr.* **50**, 333 (1994).
- <sup>12</sup>A. Ya. Faenov, I. Yu. Skobelev, S. A. Pikuz, G. A. Kryrala, J. A. Gobble, K. D. Fulton, J. Abdallah, and D. P. Kilcrease, *Phys. Rev. A* **51**, 3529 (1995).
- <sup>13</sup>Y. Aglitskiy, F. G. Serpa, E. S. Meyer, J. D. Gillaspay, C. M. Brown, A. Ya. Faenov, and T. A. Pikuz, *Phys. Scr.* (in press).
- <sup>14</sup>F. J. Currell, J. Asada, K. Ishii, A. Minoh, K. Motohashi, N. Nakamura, K. Nishizawa, S. Ohtani, K. Okazaki, M. Sakurai, H. Shiraishi, S. Tsurubuchi, and H. Watanabe, *J. Phys. Soc. Jpn.* **65**, 3186 (1996).
- <sup>15</sup>N. Nakamura, J. Asada, F. J. Currell, T. Fukami, T. Hirayama, K. Motohashi, T. Nagata, E. Nojikawa, S. Ohtani, K. Okazaki, M. Sakurai, H. Shiraishi, S. Tsurubuchi, and H. Watanabe, *Phys. Scr.* **T73**, 362 (1997).
- <sup>16</sup>H. Watanabe *et al.*, *J. Phys. Soc. Jpn.* **66**, 3795 (1997).
- <sup>17</sup>Idaho National Engineering Laboratory and Princeton Electronic Systems, Inc.
- <sup>18</sup>B. M. Penetrante, J. N. Bardsley, M. A. Levine, D. A. Knapp, and R. E. Marrs, *Phys. Rev. A* **43**, 4873 (1991).
- <sup>19</sup>F. J. Currell, J. Asada, T. Fukami, H. Hirayama, N. Nakamura, K. Motohashi, E. Nojikawa, K. Okazaki, S. Ohtani, M. Sakurai, H. Shiraishi, S. Tsurubuchi, and H. Watanabe, *Phys. Scr.* **T73**, 371 (1997).
- <sup>20</sup>H. Tsunemi, Shin'ichi Kawai, and K. Hayashida, *Jpn. J. Appl. Phys., Part 1* **30**, 1299 (1991).
- <sup>21</sup>P. Beiersdorfer, V. Decaux, S. R. Elliott, K. Widmann, and K. Wong, *Rev. Sci. Instrum.* **66**, 303 (1995).
- <sup>22</sup>P. Beiersdorfer, A. L. Osterheld, V. Decaux, and K. Widmann, *Phys. Rev. Lett.* **77**, 5353 (1996).
- <sup>23</sup>P. Beiersdorfer *et al.*, *Phys. Rev. A* **37**, 4153 (1988).
- <sup>24</sup>C. T. Chantler, D. Paterson, L. T. Hudson, F. G. Serpa, J. D. Gillaspay, and R. D. Deslattes, *Phys. Scr.* **T73**, 87 (1997).
- <sup>25</sup>G. Herrmann, *J. Appl. Phys.* **29**, 127 (1958).
- <sup>26</sup>T. E. Cowan, C. L. Bennett, D. D. Dietrich, J. V. Bixler, C. J. Hailey, J. R. Henderson, D. A. Knapp, M. A. Levine, R. E. Marrs, and M. B. Schneider, *Phys. Rev. Lett.* **66**, 1150 (1991).
- <sup>27</sup>H. Adler, E. S. Meyter, F. G. Serpa, E. Takacs, J. D. Gillaspay, C. M. Brown, and U. Feldman, *Nucl. Instrum. Methods Phys. Res. B* **98**, 581 (1995).